Automotive Experiences
Vol. 5 No. 3 (2022) pp. 355-370
p-ISSN: 2615-6202 e-ISSN: 2615-6636

Research Paper

# Aerodynamic Characteristics of Ahmed Body with Inverted Airfoil Eppler 423 and Gurney Flap on Fastback Car

**Zainal Arifin[1], Suyitno[1], Dominicus Danardono Dwi Prija Tjahjana[1], Wibawa Endra Juwana[1], Rendy Adhi Rachmanto[1], Chico Hermanu Brillianto[2], Ubaidillah[1], Singgih Dwi Prasetyo[1], Arinal Falah Muhammad[1], Mohd Afzanizam Mohd Rosli[3]**

[1]Department of Mechanical Engineering, Faculty of Engineering, Universitas Sebelas Maret, 57126, Indonesia
[2]Department of Electrical Engineering, Faculty of Engineering, Universitas Sebelas Maret, 57126, Indonesia
[3]Department of Mechanical Engineering, Faculty of Engineering, Universiti Teknikal Malaysia Melaka, 76100, Malaysia

zainal_arifin@staff.uns.ac.id

https://doi.org/10.31603/ae.7067

Check for updates

Published by Automotive Laboratory of Universitas Muhammadiyah Magelang collaboration with Association of Indonesian Vocational Educators (AIVE)

*Article Info*
*Submitted:*
06/05/2022
*Revised:*
05/06/2022
*Accepted:*
06/06/2022
*Online first:*
19/06/2022

## Abstract

The installation of aerodynamic devices, such as rear wings with the application of a Gurney flap, is very important to improve the performance of vehicles and can generate downforce and reduce slip when a car turns and brakes. The goal of this study was to determine the aerodynamic characteristics of the addition of a rear wing using an Eppler 423 airfoil, which was applied with a Gurney flap featuring variations in the angle of attack and the height of the Gurney flap. The rear wing was mounted on the Ahmed body with a rear slant angle of 15°, which is similar to the configuration on a fastback type car. This research was conducted by 3D modeling through computational fluid dynamics (CFD) simulation using ANSYS Student R18.2 by using ahmed body design. There are three variations in the angle of attack for the rear wing (0°, 7.5°, and 15°), as well as five variations in Gurney flap height of 0%, 0.5%, 1%, 1.5%, and 2% for the chord-line length. In this study, the best variation was found at an angle of attack of $15^0$ with a height of 2% C. From this configuration improved CL/CD ratio by 25.36% when compared to the results without a Gurney flap.

**Keywords:** Aerodynamic; Gurney flap; Computational fluid dynamics

## 1. Introduction

Along with the rapid development of automotive technology, the performance of four-wheeled vehicles is expected to increase. This increase in car performance is expected to be felt in every car that is distributed on the marketplace as a fastback type. This type of car has the smallest wake area, as shown in **Figure 1**, giving this type of car the lowest drag coefficient [1]. It is expected that this type of car can be driven at a high speed and acceleration, with excellent fuel efficiency [2]. Many solutions have been proposed, such as modifying the exterior of the car to improve the aerodynamic characteristics of the car's gliding state, turning stability, and energy savings [3].

Aerodynamics play an important role in achieving maximum car performance and affect safety by increasing stability and reducing fuel consumption. Therefore, it is important to pay attention to the aerodynamic characteristics of a car [4], [5]. In aerodynamics, the drag force and downforce must be considered [6]. Downforce is the force of the air fluid that presses on the top side of the car so that the wheels always rub against the ground or asphalt, thereby reducing the occurrence of slippage between the wheels and the asphalt/soil at high speeds [7]. Car performance will increase if the resulting downforce is high. Drag force is the thrust caused by the air fluid flowing in the opposite direction to the vehicle's speed. In contrast to the downforce

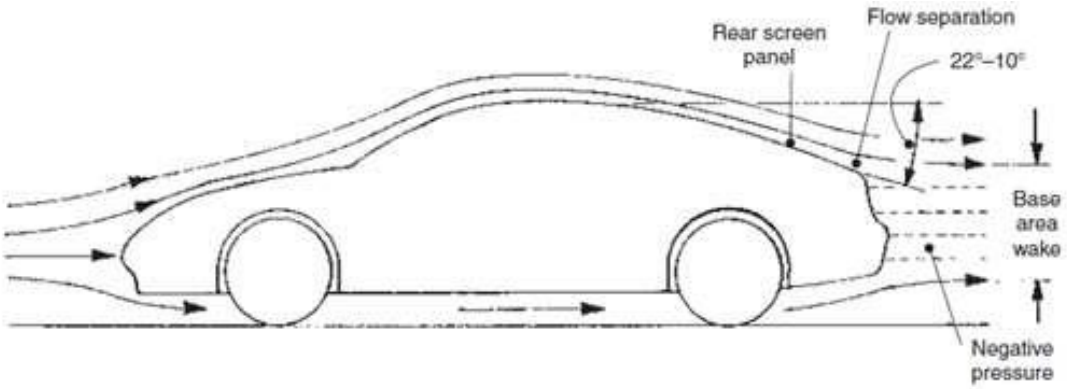


**Figure 1.** Streamline on fastback-type cars [8]

a car's aerodynamic performance will decrease if the value of the drag force is high [9].

The installation of aerodynamic devices will improve the aerodynamic aspects of the car because such devices can reduce drag force and increase downforce [10]. The addition of a rear wing on the car is a good choice because a rear wing can increase the desired aerodynamic characteristics. A rear wing is often chosen because the shape of the car has aesthetic value [11]. The rear wing usually has a variety of airfoil shapes that vary according to the required characteristics. The airfoil capability on the rear wing could be improved by adding a Gurney cover to the trailing edge of the airfoil [11]. A Gurney flap is a short flat plate measuring 0.5% to 2% of the chord-line length mounted on the trailing edge perpendicular to the chord line (Airfoil **Figure 2**) . The addition of a Gurney flap can increased the lift coefficient and reduced the drag coefficient at the same time, thereby increasing the speed when moving straight or turning [12]. Katz and Largman investigated racing-car wings with addition of a Gurney flap and reported that 5% chord Gurney flap significantly increased the lift above the baseline airfoil by about 50% [13], [14].

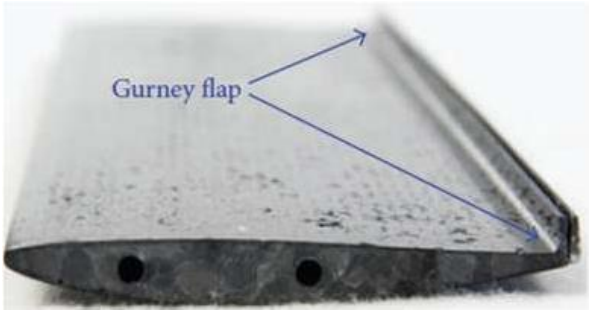


**Figure 2.** Airfoil with Gurney flap [6]

The Gurney Flap is mounted on thicker ailerons the drag can be reduced because the vortices break off further downstream on the profile, keeping the boundary layer attached and stable for a wider incidence and ground height range with respect to the baseline case [15]. In several experimental works, the geometrical data of the GF have been optimized according to the application [16]–[18]. Experimental analysis using hot anemometers has shown that the wing without a Gurney Flap has a wake with less instabilities with respect to the case including it [19], [20]. These studies indicate that although the flow downstream of the Gurney satisfies Liebeck's hypotheses [21], its instantaneous structure consists of a vortex shedding. It has been shown that for a given incidence and height of the Gurney Flap, the low pressure acting on the Gurney base remains constant along the surface. There are several studies which discuss a driver's response to side wind and a vehicle's side wind sensitivity [22]. These studies referred to cases when there was limited time for the additional downforce to be generated.

Extensive aerodynamic analyses on the profile in ground effect have been performed and the simulation of the vortex shedding from the Gurney Flap has been discussed [23]; a criterion to quantify the wake and the recirculation zone in the vortex shedding mechanism has been developed [24]. The accuracy in numerical prediction of unsteady flows is essential for the vortex shedding mechanisms, but also for other aerodynamic problems like tonal noise or vibro-acoustic stability analysis [25], [26]. In this study, we added a rear wing to a fastback-type car using an Eppler 423 airfoil with variations in the airfoil slope and Gurney flap height at high speeds. We

applied Ahmed body modelling geometry to simplify a fastback type car with simulation 3D Computational fluid dynamics (CFD) modelling applications using ANSYS Student R18.2. In this study, a comparison of cars using the Gurney Flap was obtained and also compared the model from this study with other existing studies [27]–[29].

## 2. Methodology

For the simulation 3D CFD modelling in this study, we used a laptop with an Intel R Core TM i7-5500U CPU (clock speed 2.4-3.0 GHz), 16.0 GB of RAM, Windows 10 Pro 64-bit, and a 258 GB SSD. The Fusion 360 software was used to design the Ahmed body for validation and modelling the rear wing. The ANSYS software was used to simulate the results of modelling in Fusion 360. As a solver, we used ANSYS Fluent to simulate the fluid flow in internal and external forms [30] and employed airfoil tools to create coordinate geometry based on the type of airfoil. For the simulation model with the Ahmed body and rear wing, the model was designed in 3D (IGS format) using Fusion 360. The research procedure is shown in the flow chart presented in **Figure 3**. A data converges if the error continuity, epsilon, k, x velocity, y velocity, and z velocity are below $10^{-3}$.

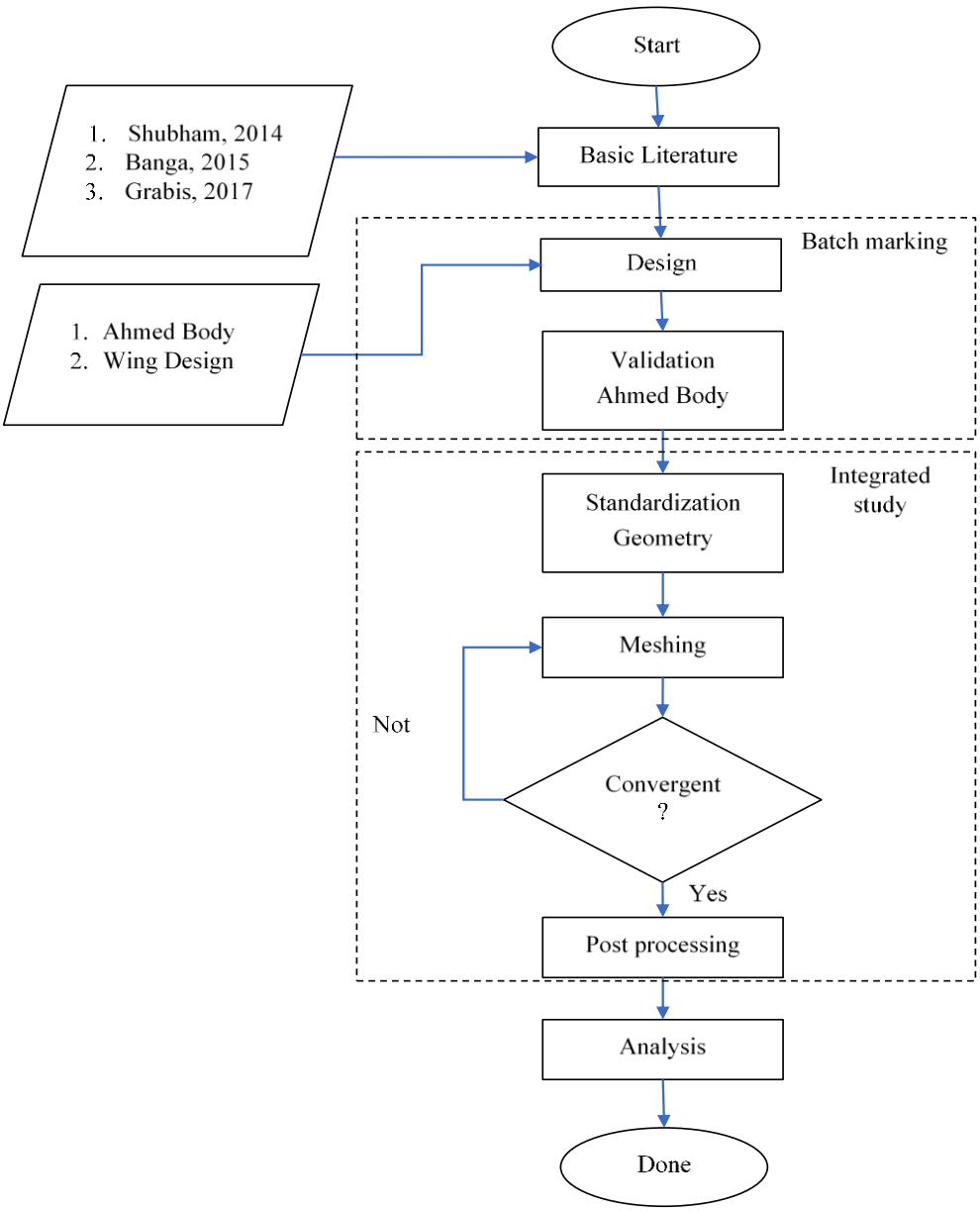


**Figure 3.** Research flowchart

### 2.1. Design

The modelling process began by designing the Ahmed body using general dimensions with a rear slant of 15°. Once validated, we added a rear wing with two endplates and one airfoil to the Ahmed body. The airfoil was designed using an Eppler 423 based on Grabis' research [31]. The rear wing was designed with 2 variations featuring angles of attack of 0°, 7.5°, and 15° along with variations in Gurney flap height of 0%, 0.5%, 1%, 1.5%, 2%. **Figure 4** and **Figure 5** provide images of the rear wing design.

**Figure 4.** 3D model of the rear wing

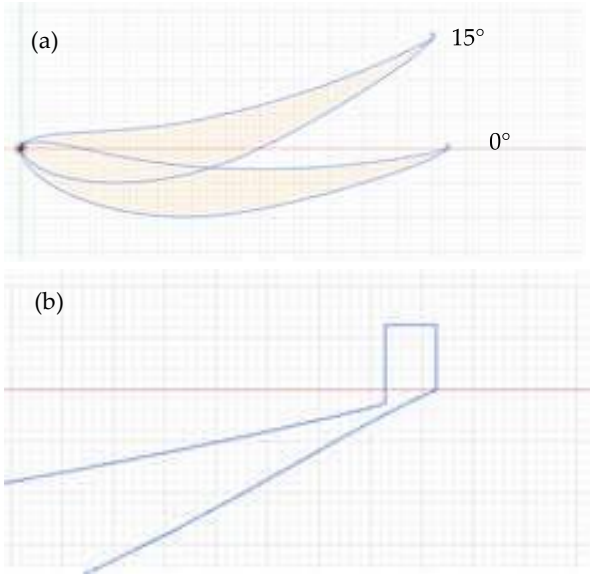


**Figure 5.** Sketch of the (a) Airfoil Eppler 423 (b) Gurney flap

After the rear wing design was completed as shown in **Figure 4** and **Figure 5**, the Ahmed body was connected to the rear wing using two cylinder rods. **Figure 6** illustrates a combination of the rear wing and Ahmed body.

### 2.2. Validation

For the validation in this study, we used an Ahmed body with a 15° rear slant, as shown in **Figure 7**. The Ahmed body is a 3-dimensional model. An Ahmed body is generally used to validate land-vehicle research because this type of body has a simple model and is able to provide accurate validation values [32]. The validation in this study is based on the research of Banga, who simulated an Ahmed body with variations in the rear slant angle at a speed of 40 m s^-1. At a rear slant angle of 15°, the drag and lift coefficients obtained were 0.24683 and 0.18501 [33]. The results of several previous studies were used as a reference and reference in identifying the ahmed body used in the subsequent research process [34], [35].

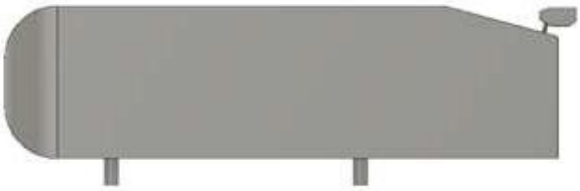

**Figure 6.** Combination of the rear wing and Ahmed body

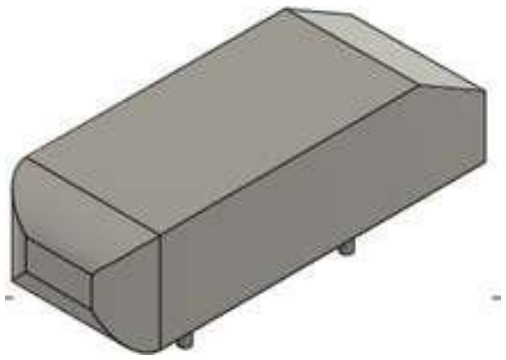

**Figure 7.** Ahmed body model with a 15° rear slant

### 2.3. Boundary Condition

The boundary conditions for modelling the Ahmed body following Banga's research included uniform velocity at the inlet and uniform pressure at the outlet, as well as symmetry around the ZY axis. The limit conditions were set as an inlet velocity of 40 m s^-1, a turbulent intensity of 1%, and a turbulent viscosity ratio of 10 at the inlet, as well as a turbulent intensity of 5% and a turbulent viscosity ratio of 10 at the outlet. The fluid density was set as 1,225 kg/m$^3$, the temperature was 288,16 K, and the viscosity was 1,789e-0.5 kg/ms. The solution methods included

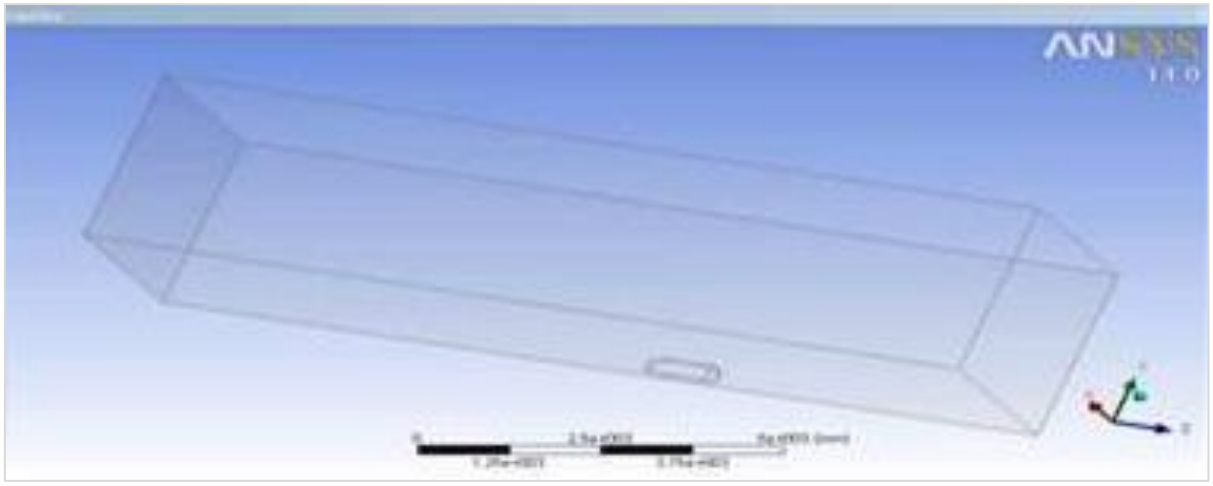

**Figure 8.** Single air body domain [33]

coupling, least-square cells, standard pressure, turbulence dissipation in the first 100 iterations, and first-order upwind, followed by second-order upwind in the next 500 iterations. The turbulence viscosity factor was set as 0.8 in the first 100 iterations and 0.95 in the next 500 iterations (**Figure 8**) [33].

The enclosure domain used to make the enclosure was based on the model length reference (L) in Madharia's research. Here, the length of the enclosure to the front surface of the front model is 2.4 L, the back is 6.6 L, the top is 1.5 L, and the width is 2L [36]. The enclosure model can be seen in **Figure 9**.

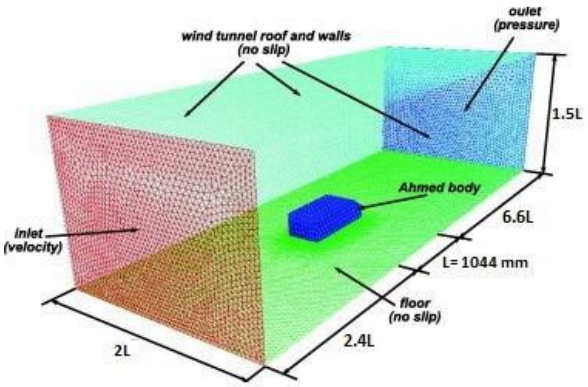


**Figure 9.** Enclosure model [37]

### 2.4. *Meshing*

The meshing is based on Banga's research and involved 3 main components: detail mesh, sizing, and name selection. Detail mesh was used to determine the meshing parameters in the model. The mesh details included the following: relevance center : coarse, smoothing : high, transition : slow, initial seed : Active assembly, min. size: 1 mm, max size : 250 mm, advanced size function : and proximity [33].

Here, sizing was done in areas that would have the greatest effect on drag and lift. Sizing was divided into two parts: face sizing and body influence. These areas are located on the wheels with limited meshing of 2 mm and on the Ahmed body with limited meshing of 10 mm. The body influence refers to the addition of a body that will affect the details of the meshing. The body influence on the Ahmed includes the wake box, underbody box and car box. A wake box was added to the rear slant area, which has a major influence on wake and flow separation. An underbody box was added to the wheel area, and a car box was added to cover the Ahmed body. The sizing limit of the meshing car box was set as 15 mm, with 10 mm for the wake box and 10 mm for the underbody box. The dimensions of the car box were (500x2350x350) mm, those of the wake box were (360x750x250) mm, and those of the underbody-box were (50x1100x200) mm. The influence of body influence can be seen in **Figure 10**.

Giving a name at the time of meshing will affect the work on a given surface. For example, the XY axis here is named symmetry so that simulations can be carried out on only half of the Ahmed body, while the other parts are assumed to be the same. This configuration will affect the effectiveness of the meshing process to reduce processing time. **Figure 9** shows that the size of the body influence towards the center is reduced and close to the initial conditions with a size of 250 to 10 mm, which indicates an increase in accuracy.

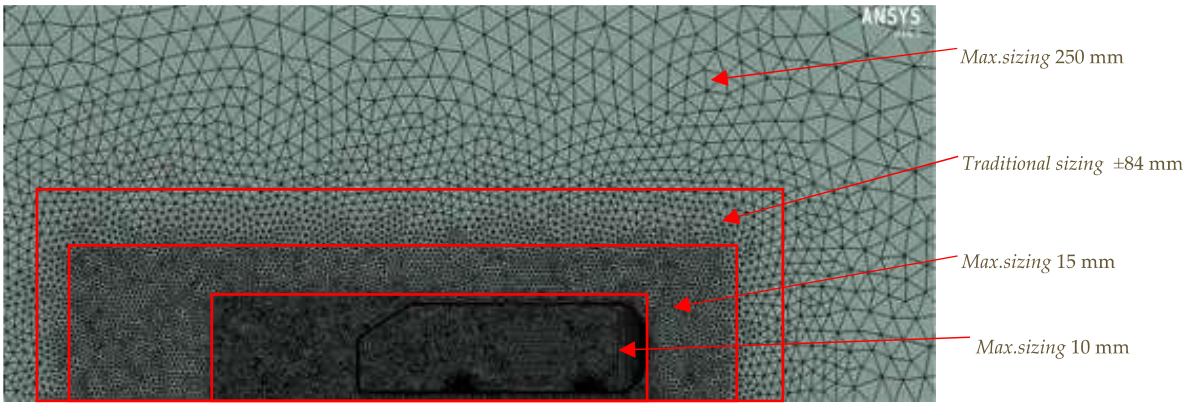


**Figure 10.** Body influence on the Ahmed body

### 2.5. *Aerodynamic Simulation on Rear Wing*

#### 2.5.1. *Boundary conditions*

The data used here are identical to those used for fastback-type cars such as Honda City cars, which generally measure 4.39 m in size. Thus, the Ahmed body magnification must be 4.2 times to obtain simulation results that are close to the same situation. Because the scale was enlarged, the scale was re-validated to produce the same $C_L$ and $C_D$ values provided in Banga's research. The Ahmed body featured a reduced speed of 4.2 times to 9.524 m s^-1 because it was assumed that the Reynolds number of the Ahmed body was the same as the Reynolds number after the scale was enlarged, assuming the same kinematic viscosity of 14.61 x 10-6 $m^2$s^-1. The body was scaled up as shown in **Figure 11**.

#### 2.5.2. *Ahmed Body's Analize*

In this study, enlargement of the Ahmed body's size and the domain of the enclosure were based on the research rules of Madhaira [36]. The body size adjustment was influenced by the Ahmed body, such as wake boxes, underbody boxes, and car boxes. The mesh size applied after magnification was 4.2 times larger than the mesh size on the standard Ahmed body. The size limit of the car box in the meshing process was 62 mm, that of the wake box was 42 mm, and that of the underbody box was 42 mm. The maximum and minimum size limits also changed to 1000 and 3 mm. This size change brought the number of elements generated to approximately 2.6 million.

After adjusting the domain enclosure size and body influence, the addition of a rear wing at the rear of the car was considered to increase the accuracy of the wing and Gurney flap. Thus, the body influence on the rear wing and Gurney cover was simulated, as shown in **Figure 11** and **Figure 12** (the body influence was (440x700x900) mm and the Gurney cover box was (10x10x750) mm). The size limit for the wing box was 34 mm, and that of the Gurney flap box was 2.52 mm due to the small size of the Gurney flap. The number of elements generated was approximately 3 million after the addition of body influence. The following provides an image of the meshing effect after adding the body influence.

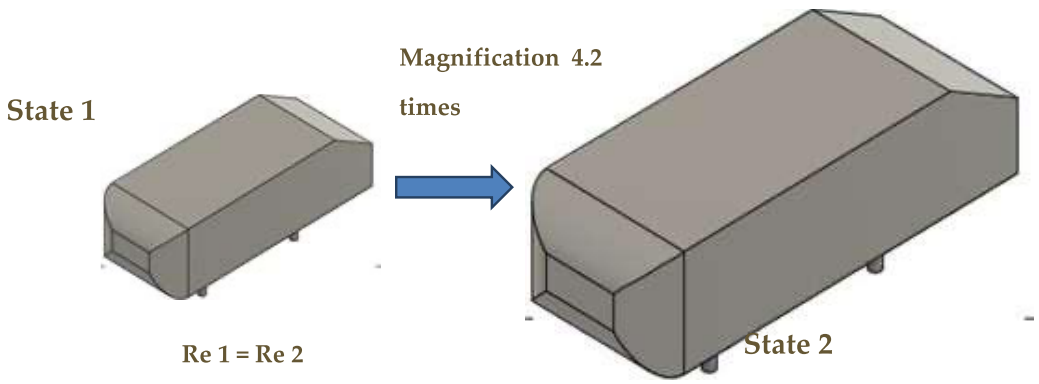


**Figure 11.** Body scaled up

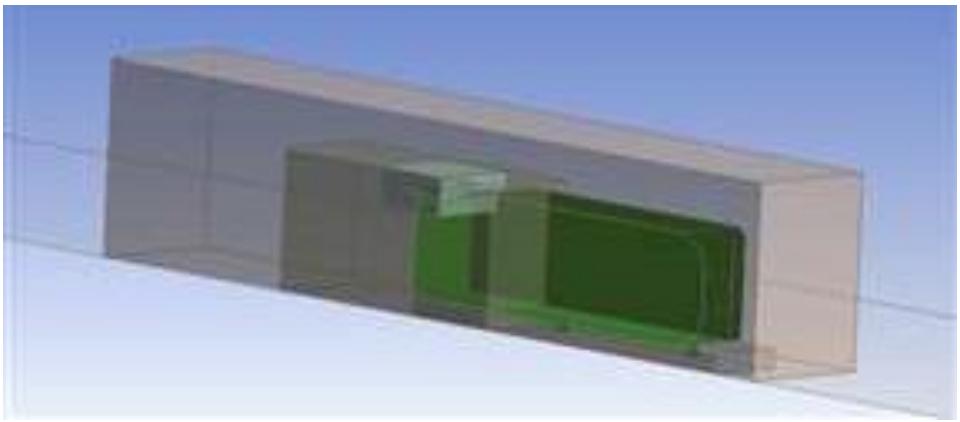

**Figure 12.** Body influence on the model

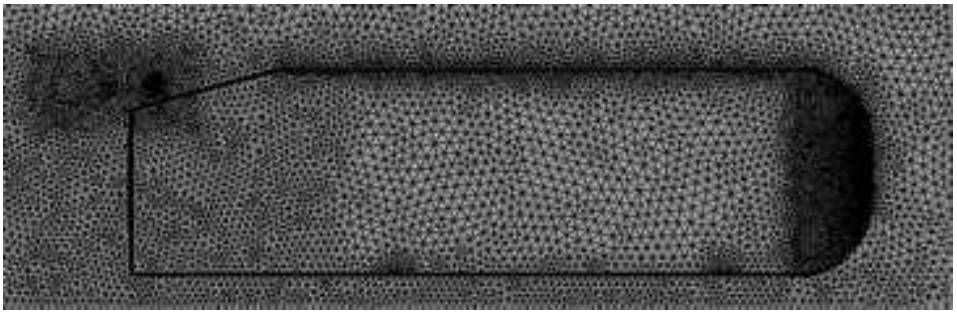

**Figure 13.** Body influence on meshing

## 3. Result

### 3.1. Design Results

The shape of an object passed by a fluid greatly affects that object's aerodynamics. From among several types of high-lift airfoils, the Eppler 423 airfoil was chosen. This airfoil was chosen because of its high downforce value [31]. Gurney flap application was also performed to increase the effect of downforce on the car without having to increase the load of the car. However, the addition of a wing with a Gurney flap also added drag force to the car. Therefore, the purpose of the wing design with a Gurney flap on the car was to maximize downforce with minimum additional drag force. To obtain the smallest possible $C_L$ value, several variations were made in the angle of attack of the airfoil and the height of the Gurney flap. Variations were made at angles of attack of 0°, 7.5°, 15° and Gurney-flap heights of 0%, 0.5%, 1%, 1.5%, and 2% for the chord-line length. In this study, we sought the best variation with the smallest $C_L$ /$C_D$ value. Variations in the angle of the airfoil and the height of the Gurney flap are shown in **Figure 13**.

The design used in the model is based on the shape of a Honda City car. The Ahmed body used in the model has a 15° rear slant angle. Next, the Ahmed body was enlarged to match the size of a Honda City car. **Table 1** provides the general dimensions of the model to be simulated.

**Table 1.** Dimensions of the test model

| Design | Dimensions (mm) |
|---|---|
| Ahmed body Tinggi height | 1419.6 |
| Ahmed body length | 4384.8 |
| Ahmed body width | 1633.8 |
| Endplate's height | 181.14 |
| Endplate length Panjang | 320.49 |
| Thickness of the endplates | 27.75 |
| Chord-line length (C) | 289.8 |
| Airfoil Width (W) | 1420.32 |
| Airfoil height (2% chord line) | 5.796 |

### 3.2. Validation Results

In the validation process, Banga's research was used as a reference parameter. The Ahmed body was used as a validation model with a rear slant angle of 15° at an inlet speed of 40 m s^-1, a drag coefficient of 0.24683, and a lift coefficient of 0.185001 [33]. Validation was carried out to determine the exact parameters to be used in the rear wing simulation with the Gurney flap, as shown in **Table 2** and **Figure 14**.

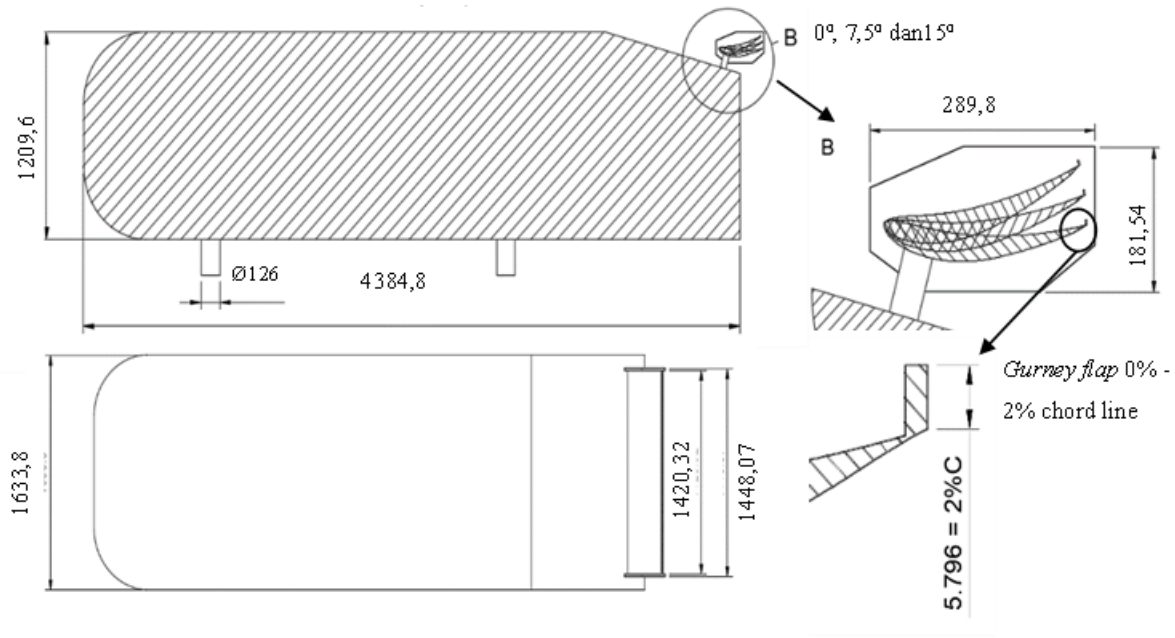


**Figure 14.** Model design results

**Table 2.** Ahmed body validation results

| Parameter | Journal [33] | Validation Results | % Error | Validation Results after scaling up | % Error |
|---|---|---|---|---|---|
| $C_L$ | 0.1850 | 0.1765 | 4.57% | 0.1905 | 2.98% |
| $C_D$ | 0.2468 | 0.2495 | 1.07% | 0.2454 | 0.57% |

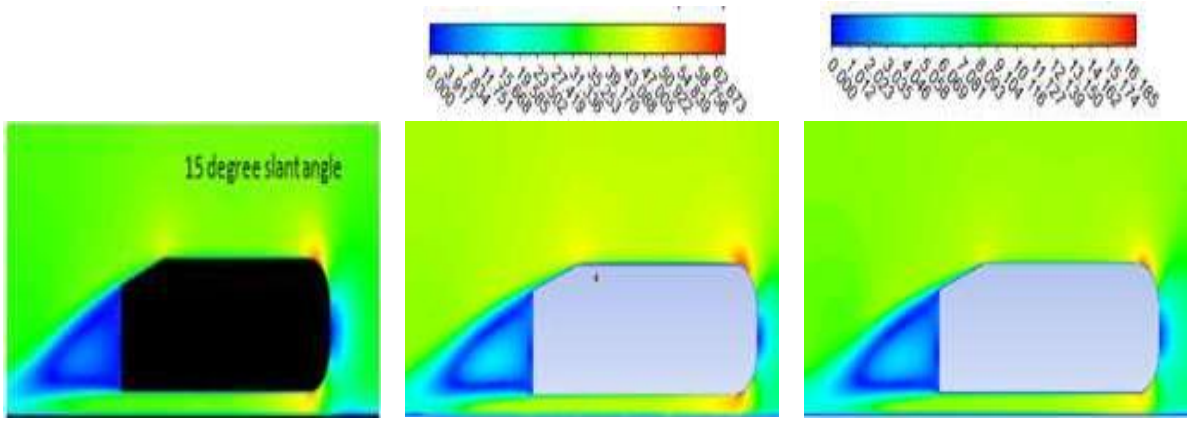


(a) (b) (c)

**Figure 15.** Velocity contours on: (a) Banga's research; (b) validation results; (c) validation results after scaling up

Table 2 shows that the results of the validation have $C_D$ errors of 1.07% and $C_L$ errors of 4.57%, while the results of validation after scaling up have $C_D$ errors of 0.57% and $C_L$ errors of 2.98%. Figure 15 presents the results of the velocity contours. Both have similar contours, with a slight difference in the wake area, which is marked in blue. In Banga's study, the wake area presented a darker blue contour colour compared to the validation results and the validation results after scaling up.

### 3.2.1. $C_L$ and Downforce Results in the Model

This simulation studied a fastback type car paired with a rear wing with a Gurney flap, with the goal to obtain the greatest possible downforce and minimum drag force, thereby reducing the slip factor and increasing the safety factor of the car, as well as increasing the car's performance when turning and braking. Simulations were carried out with angles of attack of 0°, 7.5°, and 15° and Gurney flap heights of 0%, 0.5%, 1%, 1.5%, and 2% for the chord-line length. The results of the simulations are shown in Table 3.

**Table 3.** The lift coefficient results for each test model

| Gurney flap height | $C_L$ | | | | | |
|---|---|---|---|---|---|---|
| | 0° | % Decrease | 7.5° | % Decrease | 15° | % Decrease |
| 0%C | -0.116 | - | -0.181 | - | -0.239 | - |
| 0.5%C | -0.144 | 23.23% | -0.203 | 11.97% | -0.272 | 13.67% |
| 1%C | -0.157 | 34.46% | -0.216 | 19.45% | -0.278 | 16.55% |
| 1.5%C | -0.167 | 43.35% | -0.226 | 24.79% | -0.293 | 22.43% |
| 2% C | -0.172 | 47.46% | -0.232 | 28.39% | -0.323 | 35.10% |

The highest negative lift coefficient value was observed at a 15° angle of attack with a Gurney flap of 2% C and a difference of -0.322. The lowest negative lift coefficient value of -0.116 was observed at a 0 angle of attack without a Gurney flap. Based on the data, we determined that the negative lift coefficient continued to increase as the slope of the airfoil angle of attack increased and the height of the Gurney flap increased. **Table 1** shows that the percentage decrease in the angle of attack of 0° and 7.5° tended to decrease with an increase in Gurney flap height; the opposite was observed for the slope of the 15° angle of attack, which tended to increase. **Figure 16** provides a graph of the lift coefficient for each variation of the test model.

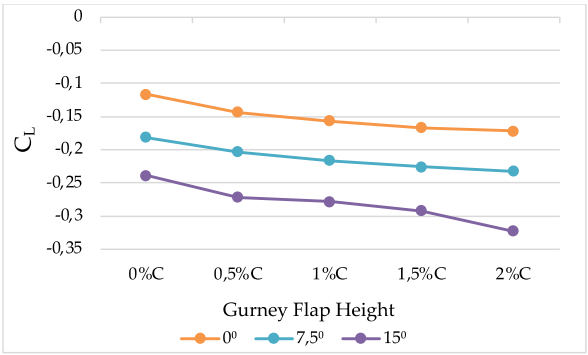


**Figure 16.** Graph of the lift coefficient for each test model

However, the 15° angle of attack presents an additional slope gradient on the graph, which means that increasing the height of the gradient affects the lift coefficient results. In this modelling test, the lift coefficient value is negative, which means that there is downforce in the body of this simulation model). Jian et al provided that lift enhancement achieving the greater heights but at the expense of increased drag. The rate of lift increment decreases for greater heights and drag. The mounting angle decreases lift and the effective area of pressure difference on the airfoil [6].

### 3.2.2. *Result of $C_D$ and Drag force in the Model*

Conventional cars that are commonly used by the public are expected to be able to drive well on both straight and winding roads. Each vehicle has its own drag force, which has a detrimental effect on the car because the drag force works in the opposite direction to the speed of the car. The greater the drag force, the greater the loss experienced by the car. Therefore, it is necessary for the value of $C_D$ on the car to be minimum to provide the best performance. **Table 4** presents the results of the drag coefficient in the simulated model.

The largest drag coefficient was possessed by the model with an airfoil angle of attack of 15°, a Gurney flap height of 2% C, and a difference of 0.322, while the smallest drag coefficient of 0.248 was possessed by the model with an airfoil angle of attack of 0° and no gurney flap. A drag coefficient graph of the research results is provided in **Figure 17**.

**Table 4.** The results of the drag coefficient for each test model

| Gurney flap height | $C_D$ | | | | | |
|---|---|---|---|---|---|---|
| | 0° | % Increase | 7.5° | % Increase | 15° | % Increase |
| 0%C | 0.248 | - | 0.266 | - | 0.299 | - |
| 0.5%C | 0.255 | 2.79% | 0.277 | 4.16% | 0.316 | 5.68% |
| 1%C | 0.257 | 3.39% | 0.286 | 7.31% | 0.318 | 6.60% |
| 1.5%C | 0.259 | 4.34% | 0.285 | 7.03% | 0.321 | 7.21% |
| 2% C | 0.263 | 5.72% | 0.294 | 10.22% | 0.322 | 7.77% |

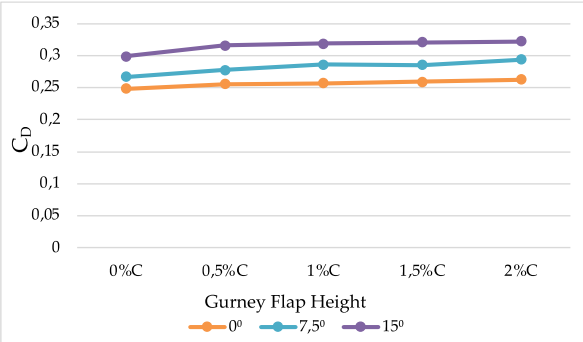


**Figure 17.** Graph of drag coefficient for each test model

As shown in **Figure 17**, the height tends to increase as the angle of attack of the airfoil increases, and the height of the Gurney flap increases. Here, the effect of increasing the value of $C_D$ will greatly affect the value of the drag force because the value of $C_D$ is directly proportional to the drag force. In the results of the drag force in the simulated model, the trendline of the drag coefficient shows that the downforce value increases with an increase in the angle of attack of the airfoil and the height of the Gurney flap. Therefore, we compared the decrease in the value of $C_L$ with the increase in $C_D$ to observe the variation that offers the best performance. A rear wing can give suitable downforce values and drag reduction by redirecting the flow of air at the right angle of approach to the wing and preventing flow separation. The drag reduction is obtained by changing the angle of attack of the airstream with the wing [38].

### 3.2.3. $C_L$ / $C_D$ Ratio Results on the Model

As shown in **Table 3** and **Table 4**, as the angle of attack of the airfoil and the height of the Gurney flap increase, the negative value of $C_L$ will increase, and $C_D$ will increase. Therefore, comparative analysis of $C_L$ / $C_D$ is important to determine the most efficient variation for fastback-type cars. The higher the value of $C_L$ / negative $C_D$ becomes, the greater the efficiency obtained. The $C_L$ data / $C_D$ in the simulated model is shown in **Table 5**.

The $C_L$ value / highest negative $C_D$ was possessed by the model with an airfoil angle of attack 15° and a Gurney flap height of 2% C with a difference of -1.002, while the $C_L$ value with the lowest negative $C_D$ of -0.469 was possessed by the model with an airfoil angle of attack of 0° and a height without a Gurney flap. At an angle of attack of 15°, the airfoil using a Gurney flap increased the $C_L$ /$C_D$ by up to 25.35% compared to the airfoil without a Gurney flap. The $C_L$ / $C_D$ value graph in this model is provided in **Figure 18**.

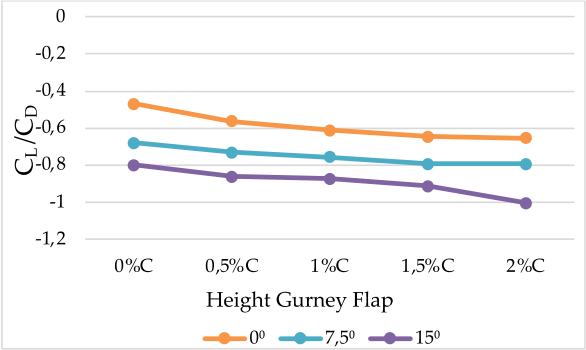


**Figure 18.** Ratio graph of $C_L$ / $C_D$ for each test model

The overall graph shows a tendency to increase. The value of $C_L$ / $C_D$ is negative, but at a 7.5° airfoil angle of attack with a Gurney flap height of 2% C, the $C_L$ value decreases. A negative $C_D$ value occurred because the value of $C_D$ increased rapidly compared to the decrease in $C_L$. Because the value of $C_L$/$C_D$ was smallest under an airfoil angle of attack of 15° and a Gurney flap height of 2% C, this variation offered the best efficiency for use in fastback-type cars.

### 3.3. Speed and Pressure Distribution Comparison

The aerodynamic characteristics of the test model were observed by analysing the velocity and pressure contours. To determine the critical area in the test model, the results of the velocity

**Table 5.** Result of the $C_L$ / $C_D$ ratio for each test model.

| Gurney flap height | $C_L$ / $C_D$ | | | | | |
|---|---|---|---|---|---|---|
| | 0° | % Decrease | 7.5° | % Decrease | 15° | % Decrease |
| 0%C | -0.469 | - | -0.679 | - | -0.799 | - |
| 0.5%C | -0.562 | 19.89% | -0.730 | 7.51% | -0.859 | 7.56% |
| 1%C | -0.610 | 30.05% | -0.756 | 11.31% | -0.874 | 9.33% |
| 1.5%C | -0.644 | 37.39% | -0.792 | 16.59% | -0.913 | 14.20% |
| 2% C | -0.654 | 39.48% | -0.792 | 16.49% | -1.002 | 25.36% |

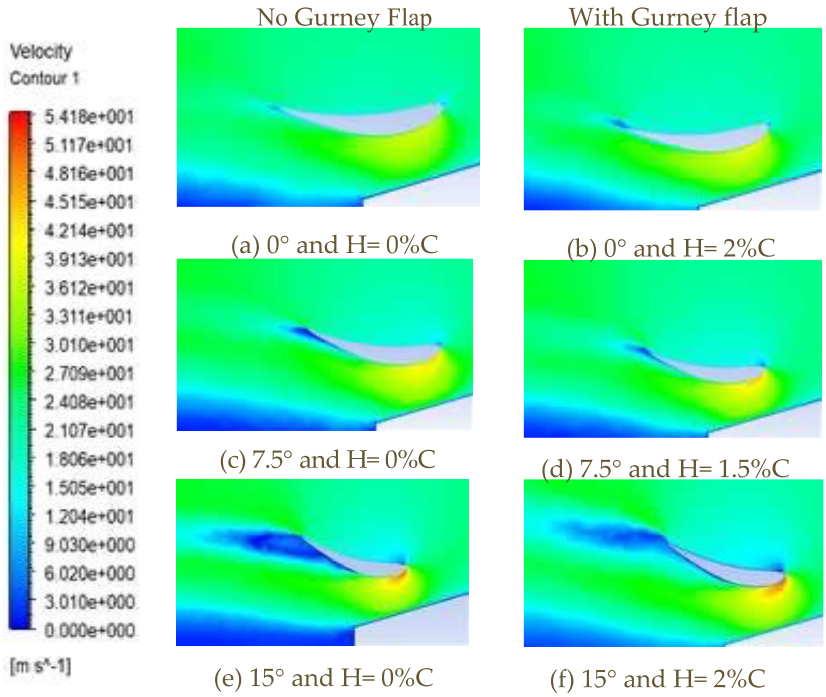


**Figure 19.** Results of the velocity contour

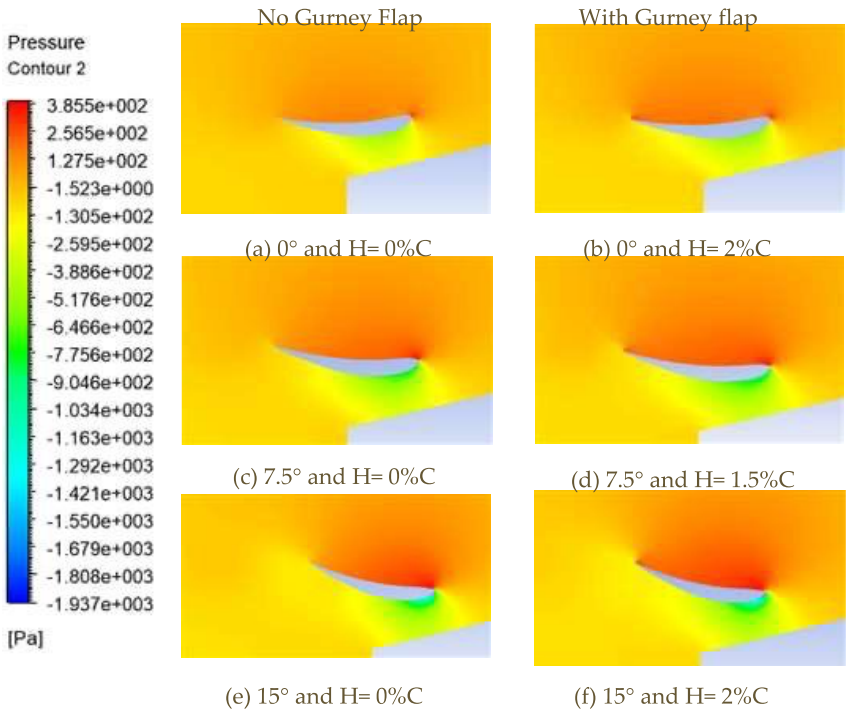


**Figure 20.** Result of the pressure contour

and pressure distribution were used to determine the contours of the area with the lowest to highest air velocity and pressure. The following are the velocity and pressure contours obtained from the simulation results at attack angles of 0°, 7.5°, and 15°; Gurney flap heights of 0%, 0.5%, 1%, 1.5%; and a 2% chord-line length.

The wing was shaped in such a way that high-speed wind moves under the wing, and low-speed wind moves through the top of the wing. It can be seen from **Figure 21** that the wind speed at the top of the wing had a lower speed than that at the bottom of the wing, which is indicated by the green contour of the top wing velocity, with a

value of 27.09 to 30.1 m s^-1. However, the lower part of the wing is marked with a yellow dominant colour contour, with a value of 39.13 to 42.14 m s^-1. On the leading edge shown in **Figure 20e** and **Figure 20f**, there is a red contour with a value of 51.17 to 54.18 m^s-1. According to Bernoulli's law, high wind speed is proportional to low pressure, and low wind speed is proportional to high pressure. **Figure 21** shows that the area above the wing features high pressure at the top. This pressure is indicated by the colour contour of orange to red, with a value of 127.5 to 388.5 Pa. At the bottom of the wing, there is a decrease in pressure, which is indicated by the colour contours from yellow to blue, with a value of -130.5 to -1808 Pa. Due to the difference in pressure at the top and bottom of the wing, downforce was observed on the rear wing. This downforce is indicated by the resulting colour contours of yellow to blue, with a value of -130.5 to -1808 Pa.

As shown in **Figure 20**, the greater the angle of attack of the rear wing is, the redder the colour contours produced at the top of the wing will be, thereby generating greater pressure. At the bottom of the wing, the results are inversely proportional; the greater the angle of attack of the rear wing is, the bluer the contour of the pressure colour will be on the leading edge of the bottom of the wing, thereby decreasing the pressure generated. Therefore, it can be concluded that the greater the angle of attack of the wing, the greater the downforce obtained.

In this study, the Gurney flap was expected to increase the ability of the wing to increase the negative $C_L$ value as much as possible with a minimum increase in the $C_D$ value. **Figure 21** shows that the Gurney flap was able to reduce the area of separation. This result can be clearly seen in the colour changes of the contours shown in **Figure 19e** with **Figure 19f**, which reduced the $C_L$ value to its greatest extent with a small increase in $C_D$. This result is demonstrated by the lowest $C_L / C_D$ value being produced in the rear-wing variation with an angle of attack of 15° and a Gurney flap height of 2% C and a difference of -1.002.

**Figure 21** shows that there was a change in the colour of the contour on the rear wing both with and without a Gurney flap installed. The wing with the Gurney flap features a redder colour contour on the top of the wing compared to the wing without the Gurney flap, especially on the leading and trailing edges. This phenomenon shows that the Gurney flap was able to increase the pressure on the top of the wing, thereby increasing the downforce on the wing.

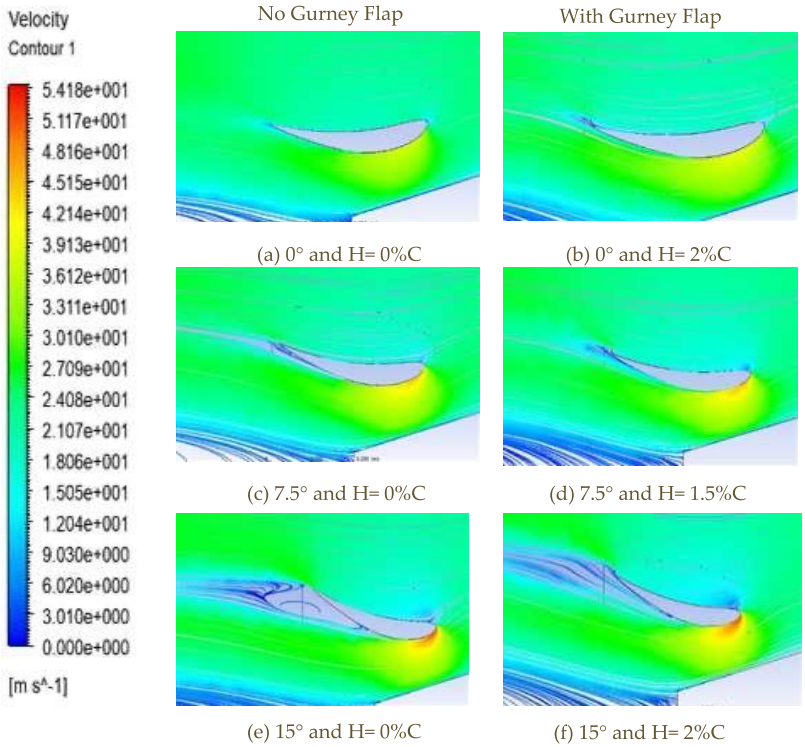


**Figure 21.** Result of the flow pattern

### 3.4. Airflow Pattern Analysis

Analysis of the air flow patterns was used to determine the shape of the flow in the test model. A streamlined flow occurs parallel to the surface of the car with a flow direction opposite to the speed of the car. The more streamlined an aerodynamic object is, the better the aerodynamics of the object will be. In addition, flow pattern analysis can be used to determine the point of separation, stall, and wake of the test model. **Figure 20** shows the results of the flow pattern on the rear wing.

Increasing the angle of attack will increase the downforce and increase the negative lift coefficient to the largest extent. When the angle of attack continues to increase, the separation from the bottom of the airfoil surface will be greater, and the separation point will move from the trailing edge to the leading edge, resulting in a decrease in the value of the negative lift coefficient.

The critical angle of attack is the angle of attack that produces the maximum negative lift coefficient. This is also known as the stall angle of attack. Conversely, above the critical angle of attack, the air will begin to slow at the bottom of the airfoil surface, and separation will begin. At a critical angle of attack, the air below the airfoil will become increasingly separated until the wing produces a maximum negative lift coefficient. When the angle of attack is increased, the separation and wake will be greater, such that the negative $C_L$ value will decrease, and the $C_D$ value will increase [31].

The application of the Gurney flap on the wing was also able to change the streamlined flow around the wing. **Figure 21e** and **Figure 21f** show that the application of the Gurney flap is able to reshape the streamlined flow that occurred at an airfoil angle of attack of 15°. This phenomenon caused a significant decrease in the $C_L$ value with a small increase in $C_D$. Thus, the variation with a 15° airfoil angle of attack with a Gurney flap height of 2% C had the lowest $C_L/C_D$.

## 4. Conclusion

In this study, the addition of a rear wing on a fastback type car with an Eppler 423 airfoil with variations in the airfoil slope and Gurney flap height at a high speed was successfully simulated. With the application of the Gurney flap, the rear wing continued to increase the downforce and drag force along with an increase in the angle of attack of the airfoil and the height of the Gurney flap. The best negative rear wing lift coefficient value was -0.322 with a drag coefficient value of 0.322. The maximum negative $C_L/C_D$ ratio was found at an angle of attack of 15° with a Gurney flap height of 2% C and a difference of -1.002. This result represents an increase of 25.35% without the Gurney flap. The percentage increase in negative $C_L/C_D$ values decreased at airfoil angles of 0° and 7.5° with the height of the Gurney flap and increased at an airfoil angle of attack of 15°. The function of a Gurney flap is to increase pressure above the wing and keep the flow under the wing from separating to increase the negative $C_L$ value with a minimum increase in $C_D$. The research of the use of various variations of rear-wing airfoils in fastback cars began to be widely developed given the large number of productions of similar cars. In addition, various developments can be applied by paying attention to the usefulness and aesthetics of fastback cars.

## Acknowledgement

This research was fully supported by a PNBP grant from the Universitas Sebelas Maret, Indonesia, with contract number 260/UN27.22/HK.07.00/2021, Penelitian Hibah Riset Grup scheme.

## Author's Declaration

### Authors' contributions and responsibilities

The authors made substantial contributions to the conception and design of the study. The authors took responsibility for data analysis, interpretation and discussion of results. The authors read and approved the final manuscript.

### Funding

PNBP grant from the Universitas Sebelas Maret, Indonesia, with contract number 260/UN27.22/HK.07.00/2021, Penelitian Hibah Riset Grup scheme.

### Availability of data and materials

All data are available from the authors.

### Competing interests

The authors declare no competing interest.

### Additional information

No additional information from the authors.

## References

[1] F. Marchesin, R. S. Barbosa, M. Gadola, and D. Chindamo, "A Road-Holding Index Based

on Ride Dynamics for High-Downforce Racing Cars," *IOP Conference Series: Materials Science and Engineering*, vol. 538, no. 1, 2019, doi: 10.1088/1757-899X/538/1/012069.

[2] D. W. Karmiadji, M. Gozali, M. Setiyo, T. Raja, and T. A. Purnomo, "Comprehensive Analysis of Minibuses Gravity Center: A Post-Production Review for Car Body Industry," *Mechanical Engineering for Society and Industry*, vol. 1, no. 1, pp. 31–40, 2021, doi: 10.31603/mesi.5250.

[3] S. Sarkar, K. Thummar, N. Shah, and V. Vagrecha, "A review paper on aerodynamic drag reduction and CFD analysis of vehicles," *Proc. A Rev. Paper Aerodyn. Drag Reduction CFD Anal. Vehicles*, pp. 231–235, 2019.

[4] A. Yudianto, I. W. Adiyasa, and A. Yudantoko, "Aerodynamics of Bus Platooning under Crosswind," *Automotive Experiences*, vol. 4, no. 3, pp. 119–130, 2021.

[5] R. P. Putra, D. Yuvenda, M. Setiyo, A. Andrizal, and M. Martias, "Body City Car Design of Two Passengers Capacity: A Numerical Simulation Study," *Automotive Experiences*, vol. 5, no. 2, pp. 163–172, 2022.

[6] S. Jain, N. Sitaram, and S. Krishnaswamy, "Computational Investigations on the Effects of Gurney Flap on Airfoil Aerodynamics," *International Scholarly Research Notices*, vol. 2015, pp. 1–11, 2015, doi: 10.1155/2015/402358.

[7] K. Kurec, M. Remer, T. Mayer, S. Tudruj, and J. Piechna, "Flow control for a car-mounted rear wing," *International Journal of Mechanical Sciences*, vol. 152, no. December 2018, pp. 384–399, 2019, doi: 10.1016/j.ijmecsci.2018.12.034.

[8] Heisler, "Advanced Vehicle Technology," *Advanced Vehicle Technology*, 2002, doi: 10.1016/b978-0-7506-5131-8.x5000-3.

[9] M. Fox, *In Reply: BEHAVIOUR THERAPY*, vol. 112, no. 483. 1966.

[10] M. Basso, C. Cravero, and D. Marsano, "Aerodynamic effect of the gurney flap on the front wing of a f1 car and flow interactions with car components," *Energies*, vol. 14, no. 8, 2021, doi: 10.3390/en14082059.

[11] G. Sivaraj, K. M. Parammasivam, M. S. Prasath, P. Vadivelu, and D. Lakshmanan, "Low analysis of rear end body shape of the vehicle for better aerodynamic performance," *Materials Today: Proceedings*, vol. 47, no. xxxx, pp. 2175–2181, 2021, doi: 10.1016/j.matpr.2021.05.521.

[12] Y. V. Yoanita, S. T. Pinindriya, E. Kumolosari, B. Gilang P, and R. Didik, "The influence of gurney flap to the stability of formula car rear wing with simulation," *Journal of Physics: Conference Series*, vol. 1823, no. 1, 2021, doi: 10.1088/1742-6596/1823/1/012064.

[13] J. Katz and L. Dykstra, "Study of an open-wheel racing-car's rear-wing aerodynamics," *SAE Technical Papers*, 1989, doi: 10.4271/890600.

[14] J. Katz and R. Largman, "Effect of 90 Degree Flap on the Aerodynamics of a Two-Element Airfoil," *Journal of Fluids Engineering*, vol. 111, no. 1, pp. 93–94, 1989, doi: 10.1115/1.3243605.

[15] L. S. Roberts, J. Correia, M. V Finnis, and K. Knowles, "Aerodynamic characteristics of a wing-and-flap configuration in ground effect and yaw," *Proceedings of the Institution of Mechanical Engineers, Part D: Journal of Automobile Engineering*, vol. 230, no. 6, pp. 841–854, Aug. 2015, doi: 10.1177/0954407015596274.

[16] G. Wahl, "918 Spyder – the impulse source for future sports car concepts BT - 5th International Munich Chassis Symposium 2014," 2014, pp. 35–56.

[17] J. Meder, T. Wiegand, and M. Pfadenhauer, "Adaptive aerodynamics of the new Porsche 911 Turbo," *ATZ worldwide*, vol. 116, no. 2, pp. 42–45, 2014, doi: 10.1007/s38311-014-0023-4.

[18] G. Estrada, "Mercedes-AMG GTR: Aerodynamics for the Record BT - Progress in Vehicle Aerodynamics and Thermal Management," 2018, pp. 135–144.

[19] D. Coles and A. J. Wadcock, "Flying-Hot-wire Study of Flow Past an NACA 4412 Airfoil at Maximum Lift," *AIAA Journal*, vol. 17, no. 4, pp. 321–329, Apr. 1979, doi: 10.2514/3.61127.

[20] B. E. Thompson and J. H. Whitelaw, "Trailing-edge region of airfoils," *Journal of Aircraft*, vol. 26, no. 3, pp. 225–234, Mar. 1989,

doi: 10.2514/3.45750.

[21] R. H. Liebeck, "Design of Subsonic Airfoils for High Lift," *Journal of Aircraft*, vol. 15, no. 9, pp. 547–561, Sep. 1978, doi: 10.2514/3.58406.

[22] C. C. MACADAM, M. W. SAYERS, J. D. POINTER, and M. GLEASON, "Crosswind Sensitivity of Passenger Cars and the Influence of Chassis and Aerodynamic Properties on Driver Preferences," *Vehicle System Dynamics*, vol. 19, no. 4, pp. 201–236, Jan. 1990, doi: 10.1080/00423119008968942.

[23] C. Cravero, "Aerodynamic Performance Prediction of a Profile in Ground Effect With and Without a Gurney Flap," *Journal of Fluids Engineering*, vol. 139, no. 3, Jan. 2017, doi: 10.1115/1.4035137.

[24] C. Cravero, N. Marogna, and D. Marsano, "A numerical study of correlation between recirculation length and shedding frequency in vortex shedding Phenomena," *WSEAS Transactions on Fluid Mechanics*, vol. 16, pp. 48–62, 2021, doi: 10.37394/232013.2021.16.6.

[25] J. E. Guerrero *et al.*, "Preliminary design of a small-sized flapping UAV: I. Aerodynamic performance and static longitudinal stability," *Meccanica*, vol. 51, no. 6, pp. 1343–1367, 2016, doi: 10.1007/s11012-015-0298-6.

[26] C. A. Niccolini Marmont Du Haut Champ and P. Silvestri, "Experimental and numerical vibro-acoustic investigation on a trimmed car door to analyze slamming event," *Applied Acoustics*, vol. 166, p. 107380, 2020, doi: https://doi.org/10.1016/j.apacoust.2020.107380.

[27] R. Salahuddin Khan and S. Umale, "CFD Aerodynamic Analysis of Ahmed Body," *International Journal of Engineering Trends and Technology*, vol. 18, no. 7, pp. 301–308, 2014, doi: 10.14445/22315381/ijett-v18p262.

[28] J. Fuller and M. A. Passmore, "The importance of rear pillar geometry on fastback wake structures," *Journal of Wind Engineering and Industrial Aerodynamics*, vol. 125, pp. 111–120, 2014, doi: https://doi.org/10.1016/j.jweia.2013.11.002.

[29] T. Avadiar, M. C. Thompson, J. Sheridan, and D. Burton, "Characterisation of the wake of the DrivAer estate vehicle," *Journal of Wind Engineering and Industrial Aerodynamics*, vol. 177, pp. 242–259, 2018, doi: https://doi.org/10.1016/j.jweia.2018.04.013.

[30] Z. Arifin, S. D. Prasetyo, A. R. Prabowo, and J. H. Cho, "Preliminary Design for Assembling and Manufacturing Sports Equipment: A Study Case on Aerobic Walker," *International Journal of Mechanical Engineering and Robotics Research*, vol. 10, no. 3, pp. 107–115, 2021, doi: 10.18178/ijmerr.10.3.107-115.

[31] M. Grabis, "Computational Fluid Dynamics Analysis of High Lift , Single Element , Inverted Airfoils in Ground Effect for an FSAE Car Front Wing Computational Fluid Dynamics Analysis of High Lift , Single Car Front Wing," 2017.

[32] O. A. Ghani, "Design Optimization of Aerodynamic Drag At the Rear of Generic Passenger Cars Using Nurbs Representation," 2013.

[33] S. Banga and M. Zunaid, "CFD Simulation of Flow around External Vehicle: Ahmed Body," *IOSR Journal of Mechanical and Civil Engineering*, vol. 12, no. 04, pp. 87–94, 2017, doi: 10.9790/1684-1204038794.

[34] I. Bayraktar, D. Landman, and O. Baysal, "Experimental and computational investigation of Ahmed body for ground vehicle aerodynamics," *SAE Technical Papers*, no. 724, 2001, doi: 10.4271/2001-01-2742.

[35] R. Varma, Mt. Scholar, and A. Professor, "CFD Analysis of Aerodynamics of Car," *International Journal of Innovative Research in Science*, vol. 7, no. 5, pp. 4689–4693, 2018, doi: 10.15680/IJIRSET.2018.0705037.

[36] P. Madharia, M. M. Tiwari, K. Ravi, and A. General, "Computational Simulation of Ahmed Body with Varying Nose radius , Ground height & Rear Slant angle," *International Journal for Research in Applied Science & Engineering Technology (IJRASET)*, vol. 3, no. 5, pp. 925–932, 2015.

[37] S. Kesarwani, Y. Jayas, and V. Chhalotre, "CFD Analysis Of Flow Processes Around The Reference Ahmed Vehicle Model," *International Journal of Engineering …*, vol. 3, no. 3, pp. 775–780, 2014.

[38] M. Palanivendhan, J. Chandradass, P. K. Bannaravuri, J. Philip, and K. Shubham, "Aerodynamic simulation of optimized vortex generators and rear spoiler for performance vehicles," *Materials Today: Proceedings*, vol. 45, pp. 7228–7238, 2021, doi: 10.1016/j.matpr.2021.02.537.